Magnetic hysteresis effects in superconducting coplanar microwave resonators

D. Bothner,* T. Gaber, M. Kemmler, D. Koelle, and R. Kleiner
Physikalisches Institut–Experimentalphysik II and Center for Collective Quantum Phenomena in LISA$^+$, Universität Tübingen, Auf der Morgenstelle 14, 72076 Tübingen, Germany

S. Wünsch and M. Siegel
Institut für Mikro- und Nanoelektronische Systeme, Karlsruher Institut für Technologie, Hertzstrasse 16, 76187 Karlsruhe, Germany

(Received 27 February 2012; revised manuscript received 31 May 2012; published 20 July 2012)

We performed transmission spectroscopy experiments on coplanar half-wavelength niobium resonators at temperature $T = 4.2$ K. We observe not only a strong dependence of the quality factor Q and the resonance frequency $f_{\rm res}$ on an externally applied magnetic field but also on the magnetic history of our resonators, i.e., on the spatial distribution of trapped Abrikosov vortices in the device. This is valid for a broad range of frequencies and angles between the resonator plane and the magnetic field direction and holds for resonators with and without antidots near the edges of the center conductor and the ground planes. In a detailed analysis, we show that characteristic features of the experimental data can only be reproduced by calculations if we assume a highly inhomogeneous rf current density and a flux density gradient with maxima at the edges of the superconductor. We furthermore demonstrate that the hysteretic behavior of the resonator properties can be used to considerably reduce the vortex-induced losses and to fine-tune the resonance frequency by the proper way of cycling to a desired magnetic field value.

DOI: 10.1103/PhysRevB.86.014517 PACS number(s): 74.25.Ha, 84.40.Dc, 03.67.Lx

I. INTRODUCTION

When Charles P. Bean introduced his model for the magnetization of hard superconductors in 1962,[1,2] he probably had not foreseen that related magnetic history effects may become of importance for circuit quantum electrodynamics,[3–5] quantum information processing,[6] or single-particle detection.[7] Of particular importance in these highly topical branches of research are superconducting coplanar microwave cavities. In many cases, the cavity quality factor Q, which defines the photon lifetime in the resonator and the sharpness of the resonance, is demanded to be rather high. Thus, there are many current efforts to identify and suppress the various energy-loss mechanisms.[8–11]

Recently, advanced hybrid systems have been proposed,[12–16] consisting of ultracold atoms, molecules, or electrons coupled to both superconducting microwave cavities and artificial atoms based on superconducting circuits. The magnetic fields required for trapping and manipulating the atomic systems[17,18] will lead to energy dissipating Abrikosov vortices,[19] adding a significant loss channel for the energy stored in the resonator. Lately, there have been different approaches to reduce the vortex-associated energy losses in particular experimental situations. In some experiments the magnetic field can be applied parallel to the plane of the superconducting film, which reduces the flux in typical coplanar resonators by orders of magnitude. This approach was used in experiments with spin ensembles, which were coupled to microwave photons in superconducting transmission line cavities.[20,21] For experiments requiring an out-of-plane magnetic field component, it has been demonstrated that losses due to vortices can effectively be reduced by trapping and pinning the flux lines either in a slot in the center of the resonator[22] or in antidots patterned at the resonator edges[23] and all over the chip.[24] Patterning with antidots is particularly suitable for zero-field cooling experimental conditions, when the vortices enter the superconductor from the edges and form a flux density gradient, called the Bean critical state. Under zero-field cooling conditions there is also a number of hysteresis effects, which on the mesoscopic scale are related to the spatial distribution of Abrikosov vortices.[25,26]

In this paper we present experimental results concerning a considerable hysteretic behavior of the characteristic quantities of coplanar superconducting resonators (with and without antidots), i.e., the quality factor Q, the loss factor $1/Q$, and the resonance frequency $f_{\rm res}$. We find that for fixed values of a perpendicularly applied magnetic flux density B, the resonator losses due to vortices $1/Q_v(B)$ can be reduced and $f_{\rm res}(B)$ can be tuned by the proper choice of magnetic history. A detailed analysis reveals strong indications that essential features of the measured hysteresis effects are best described by a combination of a highly inhomogeneous rf current distribution and field penetration models for thin films.[27,28]

The paper is organized as follows. After this introductory Sec. I we describe the sample fabrication and characterization techniques in Sec. II. In Sec. III we present and discuss our experimental data, which show a hysteretic behavior of the vortex-associated energy losses and the resonance frequency in perpendicular magnetic fields. In Sec. IV we develop a simple model to describe the dependence of the vortex-associated losses on the rf-current and vortex distribution and compare our measurements with numerical calculations. In Sec. V we discuss the possibility of exploiting the hysteresis to improve and tune the properties of the resonator in a specific magnetic field. Hysteresis effects at higher modes of the resonator and for nonperpendicular orientations between resonator plane and magnetic field are presented and discussed in Sec. VI. Finally, Sec. VII concludes the paper.

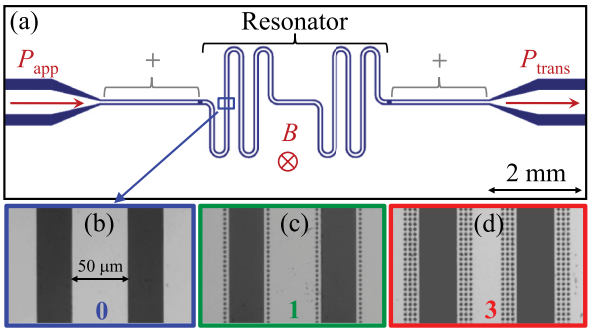

FIG. 1. (Color online) (a) Layout of 12×4 mm^2 chip with a capacitively coupled 3.3 GHz transmission line resonator. Optical images of resonators with (b) **0**, (c) **1**, and (d) **3** rows of antidots. The parts of the feedlines, which are perforated with antidots are marked with + (cf. Ref. 23).

II. RESONATOR FABRICATION AND CHARACTERIZATION

We fabricated half-wavelength coplanar transmission line resonators with a designed resonance frequency $f_{res} = 3.3$ GHz. They are capacitively and symmetrically coupled to feed lines via 90-μm-wide gaps at both ends. Due to the small coupling capacitances $C_c \approx 1$ fF[29] the resonators are undercoupled with an external quality factor $Q_c > 10^5$. Hence, the overall cavity losses in zero magnetic field and at liquid helium temperature $T = 4.2$ K are dominated by intrinsic, resistive losses. Figure 1(a) shows a sketch of the resonator layout together with optical images of the resonators without (b), with one row (c), and with three rows (d) of antidots at the edges of the center conductor and the ground planes. These resonators are denoted as Res **0**, Res **1**+, and Res **3**+, respectively, with a + indicating that also the feed lines are partially perforated, cf. Fig. 1(a). The antidots have a radius $R = 1\,\mu$m and an antidot-antidot distance $D = 4\,\mu$m. For further design considerations of the antidots regarding size and arrangement, see Ref. 23.

The structures were fabricated on a 330-μm-thick, 2-inch sapphire wafer (r-cut) by optical lithography and subsequent dc magnetron sputtering of a $d = 300$-nm-thick Nb film. After sputtering, the wafer was cut into 12×4 mm^2 chips with a single resonator. Finally, the surplus Nb was lifted-off with acetone. The transmission line has a characteristic impedance $Z_0 \approx 54\,\Omega$, where the width of the center conductor is $S = 50\,\mu$m and the gap to the ground plane is $W = 30\,\mu$m. The Nb film has a critical temperature $T_c \approx 9$ K and a residual resistance ratio $R(300\,\text{K})/R(10\,\text{K}) \approx 3.6$.

Each chip was mounted into a small brass box and the transmission line was electrically connected to subminiature-A (SMA) stripline connectors using indium as contact material. All measurements were performed at $T = 4.2$ K in liquid helium (helium-gas in the angle-dependent measurements). A magnetic field perpendicular to the resonator plane could be applied with a pair of Helmholtz coils. For angle-dependent measurements, the sample was rotated in the field of a superconducting high-field split coil. We estimate the flux density seen by the resonator to be one order of magnitude larger than the applied external field due to flux-focusing effects. As we are interested in the resonator properties at magnetic fields of some mT, no measures were taken to shield the samples from the Earth's magnetic field. Therefore, in all zero-field cooling experiments, some residual field was present, but much smaller than any field we applied (except for the angle-dependent measurements). To characterize the resonators we applied a microwave signal of power $P_{app} = -20$ dBm and frequency f to one of the feed lines and measured the frequency-dependent transmitted power $P_{trans}(f)$ with a spectrum analyzer. No attenuators or amplifiers were used. We estimate the effective power at the resonator input to be about 5–10 dB lower than P_{app}. Similarly, P_{trans} is about 5–10 dB smaller than the power directly at the resonator output.

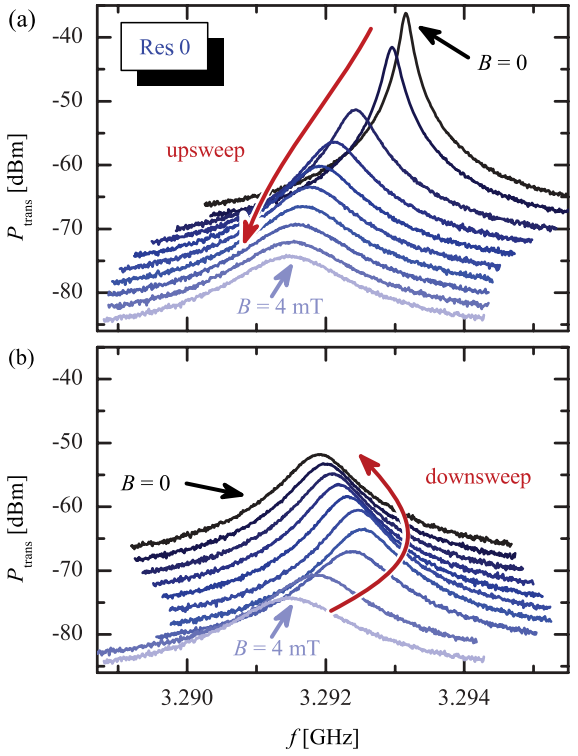

FIG. 2. (Color online) Measured transmitted power P_{trans} vs. frequency f of resonator **0** after zero-field cooling, when (a) the applied magnetic field was increased from 0 in 0.48 mT steps, with an additional curve at 4 mT and (b) B was decreased back to zero. Adjacent curves are shifted by +2 dBm for better visibility, with $P_{trans}(4\,\text{mT})$ being the unshifted reference. The applied microwave power was $P_{app} = -20$ dBm.

III. HYSTERESIS EFFECTS

Figure 2(a) shows $P_{trans}(f)$ around the fundamental mode $n = 1$ of a resonator without antidots (Res **0**) for different values of applied magnetic field between $B = 0$ and $B = 4$ mT. As reported before, we find that with increasing B the resonance frequency decreases and the resonance peak gets smaller and broader, indicating increasing losses.[19,22,23] When we reduce the magnetic field from $B = 4$ mT back to $B = 0$, we find a strong hysteresis in the resonance characteristics. Figure 2(b) depicts the corresponding spectra [for the same values of B as in (a)], showing that the original state of (a) is not restored at $B = 0$. Interestingly, $\partial f_{res}/\partial B$ changes sign at

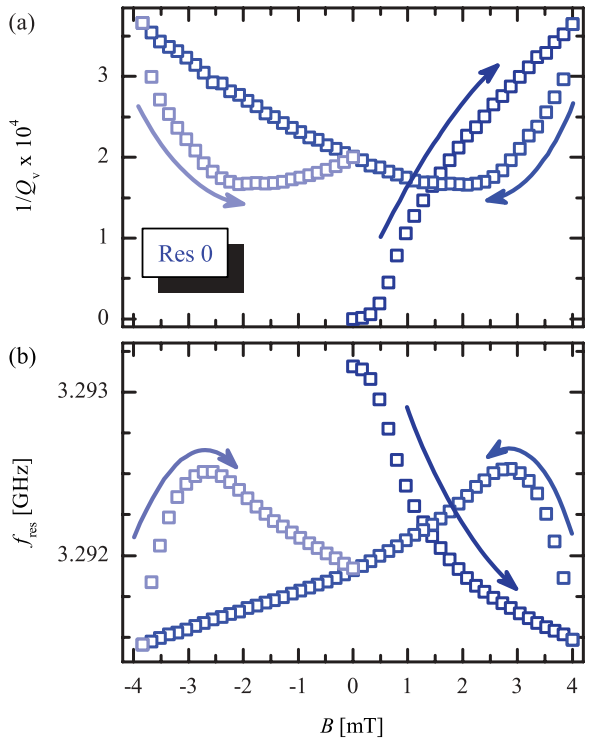

FIG. 3. (Color online) (a) Vortex associated energy losses $1/Q_v(B)$ and (b) resonance frequency $f_{res}(B)$ of the fundamental mode $n = 1$ of resonator **0** for a full cycle of B. Arrows indicate the sweep direction of the field.

$B \approx 3$ mT: After a first increase of the resonance frequency with decreasing B, f_{res} decreases again for $B \to 0$.

We fitted the measured transmission spectra with a Lorentzian and extracted the resonance frequency $f_{res}(B)$ and the full width at half maximum $\Delta f(B)$ to quantitatively analyze the hysteresis in the resonator properties. Using $f_{res}(B)$ and $\Delta f(B)$ we calculate the magnetic field-dependent quality factor $Q(B) = f_{res}(B)/\Delta f(B)$ and the magnetic field dependent losses $1/Q(B)$. In order to quantify the losses associated with the magnetic field, i.e., the presence of Abrikosov vortices, we define $1/Q_v(B) \equiv 1/Q(B) - 1/Q(0)$, cf. Refs. 19, 22, and 23. Figure 3 shows (a) the vortex associated losses $1/Q_v(B)$ and (b) the resonance frequency $f_{res}(B)$ for a full magnetic field cycle. Both $1/Q_v(B)$ and $f_{res}(B)$ show a pronounced hysteresis. Interestingly, immediately after the sweep direction is reversed at $B = 4$ mT, the losses decrease considerably and are significantly smaller than the losses for the same field values, when coming from the virgin state. In the following we indicate properties, that refer to the upsweep (downsweep) of B with $\uparrow$ ($\downarrow$). For the very first upsweep from the virgin state we use $\Uparrow$. Over a considerable range of applied magnetic field ($B \gtrsim 1.4$ mT), $1/Q_v^{\downarrow}(B) < 1/Q_v^{\Uparrow}(B)$ with a minimum of the losses $1/Q_v^{\downarrow}$ at $B \approx 2$ mT. For negative B we find a similar behavior and $1/Q_v^{\uparrow}(B) < 1/Q_v^{\downarrow}(B)$. When we repeatedly sweep the magnetic field between $\pm B_{max} = \pm 4$ mT, $1/Q_v(B)$ follows a butterfly like curve and never returns to the virgin value. This indicates that during the field cycles the sample does never return to the vortex-free state.

The resonance frequency in Fig. 3(b) shows a hysteretic behavior very similar to the losses but inverted regarding absolute values. Immediately after the sweep direction is inverted, f_{res} increases, and after reaching a local maximum it decreases again with further decreasing magnetic field. Note that the magnetic field values at the downsweep, where $1/Q_v(B)$ reaches a minimum and $f_{res}(B)$ reaches a maximum, are not equal. This discrepancy was observed for all resonators. We believe that $1/Q_v(B)$ and $f_{res}(B)$ have their extrema at different field values because the frequency shift due to a change in the kinetic inductance has not only contributions from the normal conducting vortex cores but also from the global and local screening currents, which have a slightly different distribution than the vortex cores.

Remanent vortices in type-II superconductors, observed and investigated in various studies,[25] have been reported to lead to hysteresis effects in the microwave properties of superconducting structures.[30–32] In the next section we will show that by taking a closer look at the measured hysteresis curves one can gain new insights into the underlying physics, as the particular shape of these curves is intimately related to the microwave current and vortex distribution in the resonator.

Before we proceed with the discussion and the analysis of our results, we give a rough estimate for the circulating power and the corresponding rf current density in the resonator under our experimental conditions. The power circulating in the resonator is given by $P_{circ} = 4P_{in}r(1-r)Q/\pi$ with $r = \sqrt{P_{out}/P_{in}}$.[33] Here, P_{in} (P_{out}) denotes the power at the resonator input (output) in Watt. We estimate $P_{in} = 2 \cdot 10^{-6}$ W and $P_{out} = 1.5 \cdot 10^{-8}$ W for $B = 0$. With $Q = 2 \cdot 10^4$ we find $P_{circ} = 4 \cdot 10^{-3}$ W for $B = 0$. Due to the high quality factor, P_{circ} is predominantly reactive, so the corresponding maximum current on resonance is $I \approx \sqrt{P_{circ}/(2\pi f_{res} L)}$. The total inductance $L = 2L'l/\pi^2 \approx 1.66$ nH can be calculated with the line inductance $L' \approx 424$ nH/m and the resonator length $l \approx 1.94$ cm.[34] With the center conductor cross section $A = 1.5 \cdot 10^{-7}$ cm^2 we find a current density $j = I/A = 7 \cdot 10^4$ Acm^{-2}, which is almost two orders of magnitude smaller than the critical current density of our Nb films at $B = 0$. Of course, due to uncertainties in P_{in} and P_{out}, this estimate is not very precise. However, the order of magnitude seems to be correct, as the first signs for a distortion of the Lorentzian resonance curve (indicating significant nonlinearities) appear for power levels exceeding the ones discussed here by a factor of 10^3.

IV. THE RESONATOR LOSS MODEL

In this section we introduce a simplified model that allows us to derive an approximate expression for the dependence of the vortex-associated losses $1/Q_v$ on a spatially varying flux density $\tilde{B}(x, B)$ and on the microwave current density $j^{rf}(x)$ in a superconducting coplanar resonator, cf. Fig. 4(a). B still denotes the externally applied field in y direction, and $j^{rf}(x)$ points in z direction. For simplicity we only calculate the vortex associated losses in the center conductor and discuss a possible influence of the ground planes at the end of this section.

We treat an Abrikosov vortex in the superconducting strip as a massless point-like particle under the influence of a driving Lorentz force $f_L = j^{rf}\Phi_0$ with the sheet current density $j^{rf} = j_0^{rf}\sin(\omega t)$ and a friction $f_F = \eta v$, which leads to the one-dimensional equation of motion $\eta v = j^{rf}\Phi_0$. In

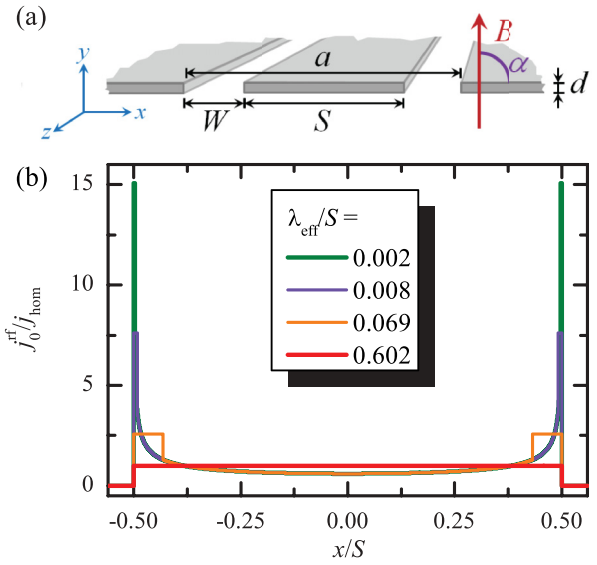

FIG. 4. (Color online) (a) Sketch of a coplanar waveguide with center conductor width S, ground-to-ground distance a, and thickness d; (b) Microwave current density distribution $j_0^{\mathrm{rf}}(x)$ normalized to the homogeneous distribution $j_{\mathrm{hom}} = I/S$ (I is the total current on the center conductor) of a coplanar waveguide for different values of λ_{eff}/S, according to Eqs. (2) and (3).

this picture the amplitude of the vortex velocity v is directly proportional to the amplitude of the alternating driving force, and we find the energy dissipated per cycle ΔE to obey the proportionality $\Delta E = \int_0^T f_L v dt \propto (j_0^{\mathrm{rf}})^2$ with $T = 2\pi/\omega$. If we have several vortices at different positions x_i with local current densities $j_0^{\mathrm{rf}}(x_i)$ we must sum up over all $\Delta E(x_i)$ from single vortices to get the overall dissipation $\Delta E_{\mathrm{total}} = \sum_i \Delta E(x_i) \propto \sum_i j_0^{\mathrm{rf}}(x_i)^2$.

The flux density $\tilde{B}(x,B)$ (divided by the flux quantum $\Phi_0 = 2.07 \times 10^{-15}\,\mathrm{Tm}^2$) can approximately be treated as a continuous representation of the vortex density in the superconductor. With this we rewrite the total dissipated energy per cycle and unit length in y direction as

$$\Delta E_{\mathrm{total}} \propto \int_{-S/2}^{S/2} |\tilde{B}(x,B)| \left[j_0^{\mathrm{rf}}(x)\right]^2 dx := \delta e(B), \qquad (1)$$

where $|\tilde{B}(x,B)|$ reflects the independence of the dissipation from the vortex polarity. $\delta e(B)$ contains all information on the spatial distributions of vortices and driving forces. It allows for a qualitative analysis of the experimentally found hysteresis curves. Within our approach, $1/Q_v(B) \propto \delta e(B)$ and the proportionality factor is eliminated below, as we only consider the normalized quantity $\delta e(B)/\delta e_{\mathrm{max}}$.

Another possibility to find the same proportionalities between δe, $j^{\mathrm{rf}}(x)$, and $\tilde{B}(x,B)$ from an electrotechnical point of view starts with the dissipated power density $p_d(x) = \mathrm{Re}[\rho_v(x)] j_0^{\mathrm{rf}}(x)^2$, which must be integrated over the width S to get the overall dissipation per unit length $D = \int_{-S/2}^{S/2} p_d(x) dx$. The hereby used real part of the vortex resistivity $\rho_v(x)$ can be obtained from the formulas given by different models.[35–37] All of these models have the linear proportionality $\rho_v(x) \propto \tilde{B}(x,B)$ in common, which again leads us to the above expression for $\delta e(B)$. This argument is closely related to the one given in Ref. 19 to obtain an expression for $1/Q_v(B)$. Interestingly, the expressions in these models are derived by treating the vortices as a vortex crystallite and not as individual particles and by adding a pinning potential. For a complete model, which provides absolute values of losses and which also considers the frequency response of the vortices, a pinning potential has to be included. However, as we are mainly interested in a qualitative understanding of the shape of the hysteresis curves, we can neglect the pinning force in the equation of motion without changing the proportionalities between $1/Q_v$, $j^{\mathrm{rf}}(x)$ and $\tilde{B}(x)$. Note that in all calculations below, we are treating $j^{\mathrm{rf}}(x)$ and $\tilde{B}(x)$ as independent quantities and discuss the justification of this assumption at the end of this section.

According to Ref. 26 and references therein, the microwave current density distribution $j_0^{\mathrm{rf}}(x)$ in the center conductor of a (flux-free) superconducting coplanar line can be approximated by

$$j_0^{\mathrm{rf}}(x) = \frac{I}{K\left(\frac{S}{a}\right) S \sqrt{\zeta(x)}}, \qquad (2)$$

where

$$\zeta(x) = \begin{cases} \frac{\lambda_{\mathrm{eff}}}{S}\left[1 - \left(\frac{S}{a}\right)^2\right], & 0 \leqslant \frac{S}{2} - |x| < \lambda_{\mathrm{eff}}, \\ \left[1 - \left(\frac{2x}{S}\right)^2\right]\left[1 - \left(\frac{2x}{a}\right)^2\right], & |x| \leqslant \frac{S}{2} - \lambda_{\mathrm{eff}}. \end{cases} \qquad (3)$$

Here, $a = S + 2W$ denotes the distance between the ground planes; in our case $a = 110\,\mu\mathrm{m}$. K is the complete elliptic integral and I is the total current. $\lambda_{\mathrm{eff}} = \lambda_{\mathrm{L}} \coth(d/\lambda_{\mathrm{L}})$ is the effective penetration depth and λ_{L} is the London penetration depth.[38,39] For $\lambda_{\mathrm{eff}}/S \ll 1$, the current distribution Eq. (2) is very inhomogeneous and has pronounced maxima at the edges of the strip. However, with increasing λ_{eff}/S the maxima continuously decrease until $j_0^{\mathrm{rf}}(x)$ becomes completely homogeneous, i.e., $j_0^{\mathrm{rf}}(x) = I/S = \mathrm{const.}$ for $\lambda_{\mathrm{eff}} \geqslant S/2$. For our samples we find $\lambda_{\mathrm{eff}} \approx \lambda_{\mathrm{L}} = 100\,\mathrm{nm}$ and $\lambda_{\mathrm{eff}}/S \approx 0.002$. Figure 4(b) shows the current distribution according to Eq. (2) for four different ratios λ_{eff}/S. For $d/S = 0.006$, as in our sample, these values correspond to $\lambda_{\mathrm{L}}/S = 0.002, 0.006, 0.02$, and 0.06. The discrete edge maxima (visible for $\lambda_{\mathrm{eff}}/S = 0.069$) are due to the particular approximation Eq. (2) for the current density: The current in the edge region of width λ_{eff} is assumed to be distributed homogeneously, while the current in the inside is independent of λ_{eff}. We have also done the calculations shown below with a different, continuous current distribution for a single superconducting strip. The results looked very similar, seeming only to require maxima near the edges. We decided to use the current distribution Eq. (2) for two reasons. First, this approximates the current density for a coplanar waveguide geometry and not only for a single strip. Second, and more important, it has inherently incorporated the transition to a homogeneous current density with increasing λ_{eff}.

To describe the magnetic flux density $\tilde{B}(x)$ in the center conductor of the resonator we start with the classical Bean profile.[1] The basic Bean model was the first model, which explained the magnetization curves of type-II superconductors on a macroscopic scale. It is thus the first choice for trying to understand our data, although technically it applies to

infinite superconducting slabs in parallel fields. The idea behind the model is that the interior of a superconductor is shielded from external magnetic fields by a macroscopic current of critical density, which continuously builds up from the surface to the interior with increasing applied field until the critical current density flows everywhere inside. Connected to the shielding current is a flux density gradient inside the superconducting sample, which according to Ampère's law is directly proportional to the critical current density. On the mesoscopic scale, the flux gradient inside the superconductor is quantized into Abrikosov vortices and the critical current density is equivalent to the depinning current density of these vortices, but this is not part of the macroscopic model. As any change in the interior flux and current state due to a change of the external fields is induced from the sample edges, the overall state of the superconductor depends on its magnetic history. During an upsweep from the virgin state, the flux density decreases linearly from the edges of the strip and can be expressed as

$$\tilde{B}^{\Uparrow}(x,B) = \begin{cases} \frac{2B^*}{S}|x| - (B^* - B), & \frac{S}{2} \geqslant |x| > \frac{S}{2}b, \\ 0, & |x| \leqslant \frac{S}{2}b, \end{cases} \quad (4)$$

where $b = (1 - \frac{B}{B^*})$, and B^* represents the applied field, when the flux fronts from both edges of the strip meet at $x = 0$. After the virgin upsweep to $B_{\max}$, the flux profile for the downsweep is given by

$$\tilde{B}^{\downarrow}(x,B) = \tilde{B}^{\Uparrow}(x,B_{\max}) - 2\tilde{B}^{\Uparrow}\left(x, \frac{B_{\max} - B}{2}\right). \quad (5)$$

The flux density profiles $\tilde{B}^{\Uparrow}(x,B)$ and $\tilde{B}^{\downarrow}(x,B)$ are shown in Figs. 5(a) and 5(b) for several values of B during (a) a field upsweep to $B_{\max} = B^*$ and (b) during the downsweep from $B = B^*$ to $B = -B^*$. Note, for each applied magnetic field B, $|\tilde{B}^{\Uparrow}(x,B)| \leqslant |B|$ and $|\tilde{B}^{\downarrow}(x,B)| \geqslant |\tilde{B}^{\Uparrow}(x,B)|$. The aforementioned relation also affects the dissipation, i.e., for the same values of applied magnetic field the losses during the downsweep should be larger than in the upsweep.

The lower part of Fig. 5 shows the calculated quantity $\delta e/\delta e_{\max}$ for the Bean model flux profile with a homogeneous [$\lambda_{\text{eff}}/S > 1$, (c)] as well as a highly inhomogeneous [$\lambda_{\text{eff}}/S = 0.002$, (d)] microwave current distribution. All calculations of $\delta e(B)$ were carried out numerically with a spatial resolution of $\Delta x = 2\,\text{nm}$. We repeated our calculations with different spacings ($1\,\text{nm} \leqslant \Delta x \leqslant 20\,\text{nm}$) and found relative deviations <3%.

In case of a homogeneous microwave current density, the dissipation only depends on the number of vortices in the sample, not on their spatial distribution, cf. Eq. (1). Starting in the virgin state, the total amount of flux increases quadratically with applied field. Therefore, $\delta e^{\Uparrow}(B)$ also has a positive curvature. As expected for this field profile (see above), $\delta e^{\downarrow} > \delta e^{\Uparrow}$ and the minimum value of $\delta e^{\downarrow}$, which corresponds to the smallest amount of flux in the sample, is reached for a negative value of applied field.

In case of a highly inhomogeneous current distribution [Fig. 5(d)] only a small region near the edges of the center conductor is responsible for almost all of the dissipation, cf. Fig. 4(b). The flux density in this area is almost identical to B, hence the hysteresis is much smaller than in the homogeneous

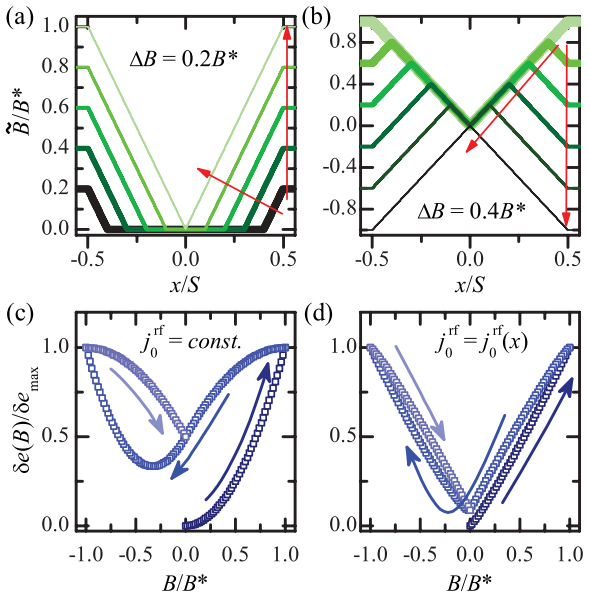

FIG. 5. (Color online) Classical Bean model flux density $\tilde{B}/B^*$ in a superconducting strip of width S during (a) the upsweep to $B = B^*$ ($B/B^* = 0.2, 0.4, 0.6, 0.8$, and 1) and (b) during downsweep from $B = B^*$ to $B = -B^*$ ($B/B^* = 1, 0.6, 0.2, -0.2, -0.6$, and -1); calculated $\delta e(B)/\delta e_{\max}$ during a magnetic field cycle $B/B^* = 0 \to 1 \to -1 \to 0$ assuming the classical Bean flux density and (c) a homogeneous as well as (d) a highly inhomogeneous microwave current density with $\lambda_{\text{eff}}/S = 0.002$. Arrows in (a) and (b) indicate the progression of the subsequent flux profiles; arrows in (c) and (d) indicate the sweep direction.

case. Although the hysteresis loop is significantly smaller, certain characteristic features of $\delta e(B)$ remain unchanged, such as the positive curvature of $\delta e^{\Uparrow}(B)$, the relation $\delta e^{\downarrow} > \delta e^{\Uparrow}$, and the fact that the position of the dissipation minimum during the downsweep is found at $B < 0$. Consequently, the classical Bean field profile does not properly describe the hysteresis as observed in our experiments.

An alternative model of the flux density distribution in thin film geometries was first considered by Norris[27] and later discussed by Brandt and Indenbom.[28] It is basically the aforementioned Bean model adapted to the geometry of thin superconducting strips in perpendicular magnetic fields. In this Norris-Brandt-Indenbom (NBI) model the flux density is given by

$$\tilde{B}^{\Uparrow}(x,B) = B_c \begin{cases} \tanh^{-1}\frac{\sqrt{(x-S')(x+S')}}{|x|\tanh(B/B_c)}, & \frac{S}{2} \geqslant |x| > S' \\ 0, & |x| \leqslant S', \end{cases} \quad (6)$$

where $S' = S/2\cosh(B/B_c)$, $B_c = \mu_0 d j_c/\pi$ is the characteristic field,[28] and j_c is the critical current density of the superconductor. Using the estimated $j_c \approx 5 \times 10^6\,\text{A/cm}^2$ of our Nb, we calculate $B_c \approx 6\,\text{mT}$. As can be seen from Eq. (6), the NBI model leads to an excess flux density at the edges of the strip compared to the classical Bean profile. The downsweep flux density $\tilde{B}^{\downarrow}(x,B)$ is again defined according to Eq. (5).

The NBI flux density profile is shown in Fig. 6(a) for several values of B during a field upsweep to $B = 3B_c$ and in Fig. 6(b) during the downsweep from $B = 3B_c$ to $B = -3B_c$. $\tilde{B}^{\downarrow}$ shows

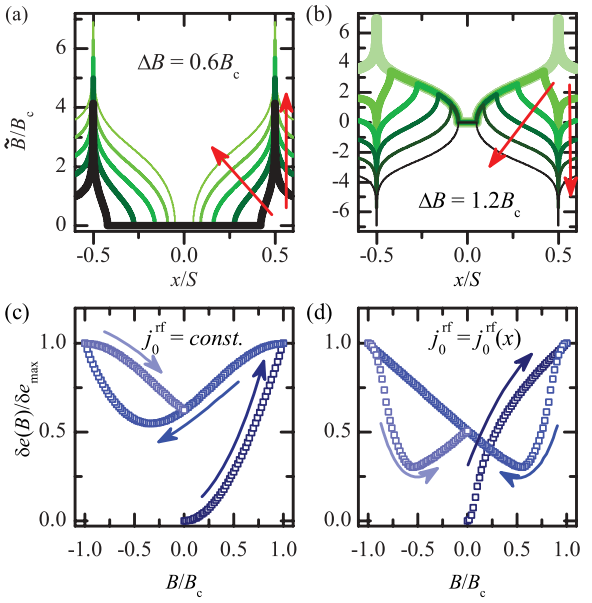

FIG. 6. (Color online) NBI model flux density $\tilde{B}/B_c$ in a superconducting strip of width S during (a) the upsweep to $B = 3B_c$ ($B/B_c = 0.6, 1.2, 1.8, 2.4$, and 3) and (b) during downsweep from $B = 3B_c$ to $-3B_c$ ($B/B_c = 3, 1.8, 0.6, -0.6, -1.8$, and -3). Calculated $\delta e(B)/\delta e_{max}$ during a magnetic field cycle $B/B_c = 0 \rightarrow 1 \rightarrow -1 \rightarrow 0$ assuming the NBI flux density and (c) a homogeneous as well as (d) a highly inhomogeneous microwave current density with $\lambda_L/S = 0.002$ and $d/S = 0.006$. Arrows in (a) and (b) indicate the progression of the flux profile, arrows in (c) and (d) indicate the sweep direction.

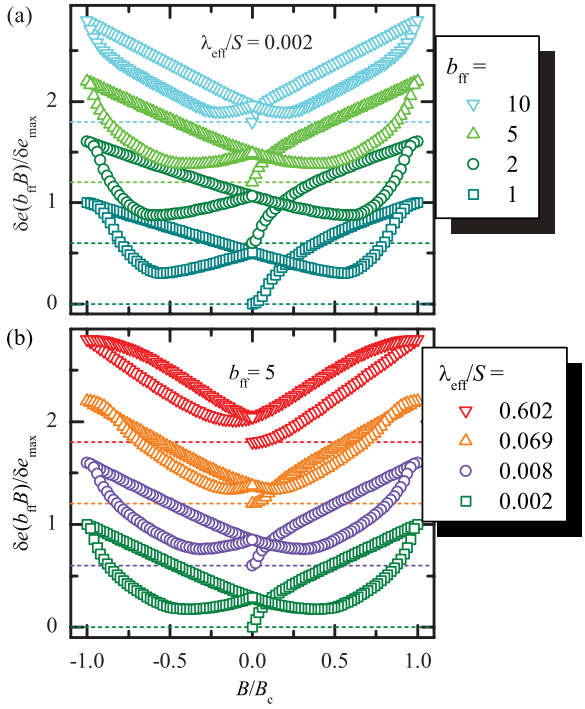

FIG. 7. (Color online) (a) $\delta e(b_{ff}B)/\delta e_{max}$ vs. external flux density B/B_c calculated for the NBI model with different flux-focusing factors b_{ff}. (b) $\delta e(b_{ff}B)/\delta e_{max}$ vs. cycled flux density B/B_c calculated for the NBI model for different ratios λ_{eff}/S. Adjacent curves are subsequently shifted by $+0.6$ for better visibility.

a remarkable behavior. For an externally applied field that is still positive, the flux density close to the edge of the thin film is already zero. When B is decreased further, $\tilde{B}^{\downarrow}$ at the film edge becomes negative and the point of zero flux density moves deeper into the sample, separating areas with antivortices from those with vortices.

To achieve comparability with experimental results, where $B_{max} = 4\,\text{mT}$, a field range of $|B| \lesssim B_c \approx 6\,\text{mT}$ was chosen for numerical calculations. Figures 6(c) and 6(d) show $\delta e(B)/\delta e_{max}$ for (c) a homogeneous and (d) a highly inhomogeneous current density. In the calculations we avoided the divergence of the NBI flux density at the strip edges by positioning them between two integration points, i.e., by effectively introducing a cutoff for $\tilde{B}$ at $\Delta x/2$ from the conductor edges. In case of $j_0^{rf}(x) = \text{const.}$, the NBI and the classical Bean model lead to similar $\delta e(B)/\delta e_{max}$ dependences, cf. Fig. 5(c), which—as already mentioned—disagree with our experimental data. For the inhomogeneous rf current distribution, however, $\delta e(B)/\delta e_{max}$ reproduces almost all characteristic features of the measured curve, cf. Figs. 3(a) and 6(d). In particular, the hysteresis loop has a butterfly like shape, where $\delta e^{\downarrow}(B) < \delta e^{\Uparrow}(B)$ for a considerable range of B. Also, $\delta e^{\Uparrow}(B)$ exhibits a predominantly negative curvature and the minimum of $\delta e^{\downarrow}(B)$ can be found at $B > 0$.

Yet, there is still a difference between experiment and theory. The slow increase of the losses at very small fields and the abrupt decrease immediately after the inversion of the sweep direction is clearly visible in experiment, but not in theory. Using the models described before, the curvatures $\partial^2\tilde{B}^{\Uparrow}(x)/\partial B^2$ at $B = 0$ and $\partial^2\tilde{B}^{\downarrow}(x)/\partial B^2$ at $B = B_{max}$ are directly linked, cf. Eq. (5). Therefore, there is always a symmetry between the first slow increase of the losses at the beginning of the upsweep and the slow decrease at the beginning of the downsweep. We believe that the asymmetry in experiment originates from the small but nonzero lower critical field B_{c1} of the superconductor, which is not included in the calculations. The existence of B_{c1} inherently leads to an asymmetry between the upsweep from the virgin state and any following sweep. The critical field value, however, at which the first vortex enters the superconductor, is not B_{c1}. It is moreover determined by the geometry of the sample and might be different for ground planes and center conductor. It also may depend on the position along the resonator.

In Fig. 7 the dependence of the hysteresis loop on the ratio λ_{eff}/S and the flux-focusing factor $b_{ff} = B_{eff}/B$ with the effective flux density B_{eff} is shown. Due to the ground planes, the flux density seen by the center conductor B_{eff} certainly is larger than the applied B. This is approximately taken into account by b_{ff}, where spatial variations of B_{eff} are neglected. Figure 7(a) shows $\delta e(b_{ff}B)/\delta e_{max}$ for $b_{ff} = 1, 2, 5$, and 10. All curves exhibit the same essential features of the hysteresis with some minor differences. With increasing b_{ff}, the field regions around $B = 0$ and $B = B_{max}$, where curvatures of $\delta e^{\Uparrow}$ and $\delta e^{\downarrow}$ change sign, become effectively compressed. Furthermore, the position of the downsweep minimum shifts with b_{ff}. By comparing calculations with experimental data, we find best qualitative agreement for a flux-focusing factor between $b_{ff} \approx 2$ and 5. Although the estimated value of $B_c \approx 6\,\text{mT}$ is comparable to $B_{max} = 4\,\text{mT}$ in experiment and a flux-focusing

factor of $b_{ff} \approx 5$ seems reasonable, we would like to emphasize that the theoretical model presented in this paper is too simple to be used for a quantitative analysis of our experimental data.

Besides the flux-focusing factor, the homogeneity of the rf current distribution described by λ_{eff}/S determines the shape of the hysteresis loop. Figure 7(b) shows $\delta e(b_{ff}B)/\delta e_{max}$ for four different ratios λ_{eff}/S, corresponding to current distributions shown in Fig. 4(b). Starting from $\lambda_{eff}/S = 0.002$, which corresponds to our experimental conditions, the hysteresis loop becomes smaller with increasing homogeneity. For $\lambda_{eff}/S \approx 0.069$ hardly any hysteresis can be seen. When λ_{eff} is increased further, up- and downsweep curves do not even cross anymore.

In our calculations we have assumed that the microwave current density and the flux profile (vortex density distribution) can be treated independently from each other. In general, however, the presence of a flux gradient leads to a redistribution of the transport current and vice versa.[28] Also, the oscillation amplitude of the vortices δx is assumed to be smaller than the length scale on which the current distribution varies, such that $j_0^{rf}(x \pm \delta x) \approx j_0^{rf}(x)$. We believe that both assumptions are reasonable, as in experiment the vortex associated losses $1/Q_v$ are almost independent of the applied microwave power, as long as $P_{app} < 0\,\text{dBm}$.[23] If the microwave self-field would significantly disturb and rearrange the static magnetic field configuration, e.g., by introducing additional vortices, we would expect nonlinearities,[41] which would lead to a power dependence of the losses.

Another simplification is the field-independent flux-focusing factor. In reality b_{ff} depends on B, which is only partially focused into the gaps of the coplanar waveguide; some of the flux also penetrates the superconductor in the form of Abrikosov vortices and this amount is field-dependent. Moreover, due to the geometry of our samples with a meandering resonator line, b_{ff} is expected to vary along the resonator. Consequently, also the losses δe depend on the position along the resonator.

Finally, we have not taken into account dissipation in the ground planes. If the vortices symmetrically penetrate the ground planes and the center conductor, the presence of ground planes would not affect the shape of the hysteresis at all but only increase the absolute values of the losses due to return currents at their edges. If there is an asymmetry in vortex penetration due to different demagnetizing factors of center conductor and ground planes, this can be viewed as equivalent to different flux-focusing factors for the ground planes and the center conductor. The resulting hysteresis of the whole system with ground planes would be a mixture of two slightly different hysteretic curves like those in Fig. 7(a). The influence of the ground plane losses, however, is in any case reduced by a factor $a/S \approx 2.2$ compared to the losses in the center conductor due to the smaller current density.[42]

In the experiments all the above mentioned effects are merged together, but we think that none of them fundamentally changes the observed and analyzed hysteretic behavior.

V. DEMAGNETIZATION AND TUNABILITY

In order to explore the possibility to return to the virgin state after magnetic cycling, we performed a demagnetization procedure, i.e., we repeatedly swept the magnetic field up and down with decreasing B_{max} and monitored the corresponding resonances. The procedure slightly differs from commonly used demagnetization cycles, as we kept the sweep rate $\partial B/\partial t$ constant, i.e., the period for one field cycle decreases with decreasing B_{max}. The idea behind this procedure is based on the Bean and NBI model. Repeatedly sweeping the field up and down with decreasing B_{max} creates a sawtooth-like flux pattern in the superconductor, with a sawtooth amplitude, which depends on the difference $\Delta B_{max} = |+B_{max}| - |-B_{max}|$ between consecutive extrema (here $\Delta B_{max} = 0.16\,\text{mT}$). During each second half cycle of this procedure Abrikosov antivortices are pushed into the sample almost as far as the vortices from the half cycle before reach. The field distribution at the end resembles narrow alternating regions of vortices and antivortices, whose density is determined by ΔB_{max}.

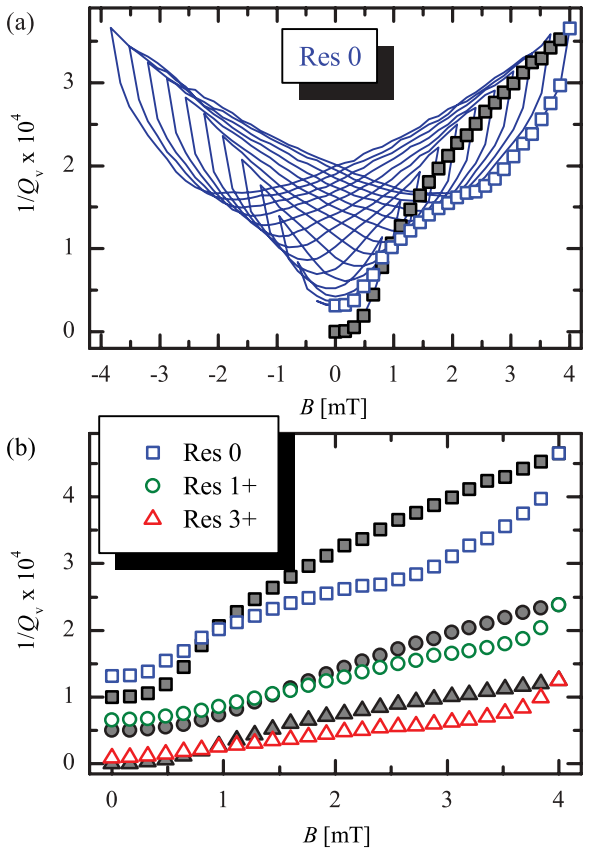

FIG. 8. (Color online) (a) $1/Q_v(B)$ of Res **0** ($n = 1$) during demagnetization (line); solid and open squares indicate the virgin field sweep and minimum values after virgin field sweep for $B \geqslant 0$, respectively; (b) $1/Q_v(B)$ of the resonators **3**+, **1**+ (hifted by $+5 \cdot 10^{-5}$), and **0** (shifted by $+1 \cdot 10^{-4}$) for the virgin field sweep (full symbols) and the minimum values after virgin field sweep (open symbols).

Figure 8(a) shows the measured energy losses $1/Q_v(B)$ during demagnetization (solid line). As can be seen with decreasing B_{max}, the losses at $B = 0$ are decreasing and approach the virgin state value. The small but finite value for $1/Q_v$ after demagnetization is probably due to the presence of remanent (anti-)vortices, which were not annihilated during

the repeated cycles. To avoid nonequilibrium effects, we waited about one minute after each field step, i.e., a full demagnetization procedure took about one day.

The demagnetization curve in Fig. 8(a) shows that over almost the whole magnetic field range ($B \geqslant 1$ mT) the envelope of the full curve after the virgin field sweep, i.e., the minimum values of the vortex associated losses (open squares), lie considerably below the values of the virgin field sweep (full squares). This provides the opportunity to significantly reduce the losses of resonators or other microwave circuitry components operated in magnetic fields (e.g., when it comes to trapping of an ultracold atom cloud in the vicinity of a resonator) by proper choice of magnetic history. We are aware that the achievable reduction is small compared to other approaches such as using antidots or slots. However, for resonators patterned with antidots our procedure can be used to additionally improve the device performance as shown in Fig. 8(b), where we plot the virgin sweep data as well as the minimum values during demagnetization for the resonators **0**, **1**+, and **3**+. Although the losses are already significantly reduced in the resonators with antidots,[23] cycling in magnetic fields can further reduce $1/Q_v$ up to 30%. As can be seen in the next section, where we explicitly show data for resonator **3**+, also the shape of the hysteresis curves seems rather independent of the presence of antidots. By consulting our simple model, we can see how this somewhat surprising independence might be explained. The reasonable assumption that the antidots increase the mean pinning force acting on the vortices, i.e., increase the critical current density j_c, leads to a higher characteristic flux density B_c in the NBI model. For the calculated hysteresis curves, an increase of B_c is equivalent to a decrease of b_{ff}, which does not considerably change the nature of the hysteresis, as long as the change of b_{ff} is not too large, cf. Fig. 7(a). In reality, of course, the situation is probably more complicated, as the relatively large antidots will modify the flux density profiles more than just globally increasing j_c and a detailed analysis would be much more difficult.

The evolution of the resonance frequency f_{res} during demagnetization is depicted in Fig. 9(a). The variation in f_{res} covers a range of $\sim$1 MHz. For a quantification, we define the frequency tunability of the resonator as the difference between the maximum and the minimum resonance frequency $t_{\mathrm{res}} \equiv f_{\mathrm{res,max}} - f_{\mathrm{res,min}}$ for each value of B. The resulting $t_{\mathrm{res}}(B)$ of the three resonators with and without antidots is shown in Fig. 9(b) for $B \geqslant 0$. For all three resonators $t_{\mathrm{res}}(B) \approx 1$ MHz, almost independent of perforation and B, with a small tendency to increase with the number of antidots.

A tunability like this might be useful, e.g., for fine-tuning a superconducting cavity to the (fixed) transition frequencies of ultracold atom clouds. As for any value of B, each f_{res} value within the tunability range is accessible by at least two different histories, and as the maxima (minima) of the frequency (loss) hysteresis are not at the same field values, one has to check all possibilities to find the optimum combination of desired frequency and losses. As the exact parameters of the hysteresis slightly differ from device to device and probably from setup to setup, we cannot give a common recipe for finding the best working point here. Instead, each device has to be precharacterized in the corresponding experimental situation.

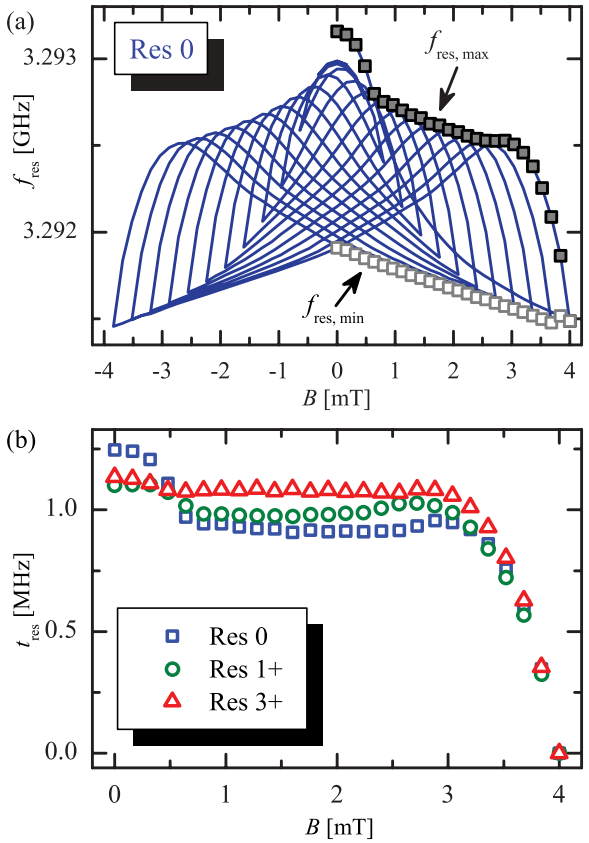

FIG. 9. (Color online) (a) Measured resonance frequency $f_{\mathrm{res}}(B)$ of Res **0** for a full demagnetization cycle (line) with maximum values (full squares) and minimum values (open squares) for positive magnetic fields; (b) Tunability $t_{\mathrm{res}}(B) = f_{\mathrm{res,max}}(B) - f_{\mathrm{res,min}}(B)$ of the resonators **3**+ (triangles), **1**+ (circles), and **0** (squares).

We emphasize that we do not propose to tune the properties of planar superconducting microwave components by just applying a magnetic field and introducing Abrikosov vortices here. If one just would like to fabricate a frequency tunable device for instance, other approaches with larger ranges and tunability velocities seem more promising.[43–45] However, if the microwave components have to be operated in specific magnetic fields anyway, magnetic history effects provide a nice additional possibility to reduce the losses and tune the resonance frequencies by spatially rearranging Abrikosov vortices.

VI. HIGHER MODES AND OTHER ANGLES

So far we have only considered the fundamental mode of our resonators and an operation in a perpendicular magnetic field. In the following we will present measurement results on higher modes and discuss the influence of the tilt angle α (cf. Fig. 4) between resonator plane and magnetic field on the hysteresis loop.

Figure 10 exemplarily shows the measured energy losses $1/Q_v(B)$ of resonator **3**+ for (a) the fundamental mode $n = 1$ and (b), (c), (d) the first three harmonics $n = 2,3,4$ in perpendicular magnetic fields. Clearly, the characteristic

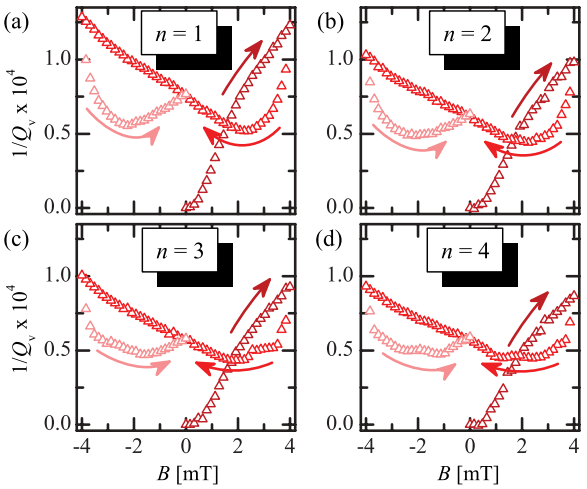

FIG. 10. (Color online) Measured vortex associated energy loss $1/Q_v(B)$ for the four lowest modes $n = 1$ to 4 of Res **3**+ for a full cycle of magnetic field.

features of the hysteresis loop can also be seen for higher modes.

Interestingly, with increasing frequency a fine structure within the hysteresis curves emerges; see, e.g., Fig. 10(d) at $B \approx \pm 1.5$ mT. This fine structure might be related to inhomogeneously distributed losses along the resonator. Depending on the resonator mode n, nodes and antinodes of the microwave current standing wave probe different parts of the resonator, i.e., they contribute differently to the overall losses. As already pointed out, there is a variation of the flux-focusing factor and, thus, the effective flux density along the resonator due to its geometry. The flux focusing is smaller in the meandering lines than in the straight part at the midpoint of the resonator, as the adjacent gaps of the meander allow for partial sharing of flux. Consequently, for different flux-focusing factors the downsweep minima might occur at different applied magnetic fields and the superposition of the $1/Q_v$ curves of several antinodes (which is what we measure) might lead to a fine structure on the hysteresis loop with multiple minima.

Figure 11 shows the measured $Q(B)$ of the fundamental mode of resonator **3**+ for three different angles. In perpendicular field, $\alpha = 90°$, we find the already described hysteresis with significantly increased Q (reduced $1/Q_v$) on the downsweep branch; see Fig. 11(a). For $\alpha < 90°$, the hysteresis loop hardly changes, as can exemplarily be seen in Fig. 11(b), where $\alpha \approx 15°$. Note that the field range is about four times larger than compared to the measurement with perpendicular orientation. The general shape of the hysteresis and the downsweep improvement in Q are very similar for both angles. As $\sin(15°) \approx 0.26$, this strongly suggests that the resonator losses are primarily determined by the component of B perpendicular to the sample.

The situation changes dramatically for $\alpha \approx 0°$, where the magnetic field was swept between ± 0.2 T, as can be seen in Fig. 11(c). For $B < 80$ mT the decrease in Q is relatively small and also reversible (not shown). When the magnetic field is increased further, the quality factor rapidly decreases. After sweep direction inversion, Q remains low until at $B \approx 50$ mT

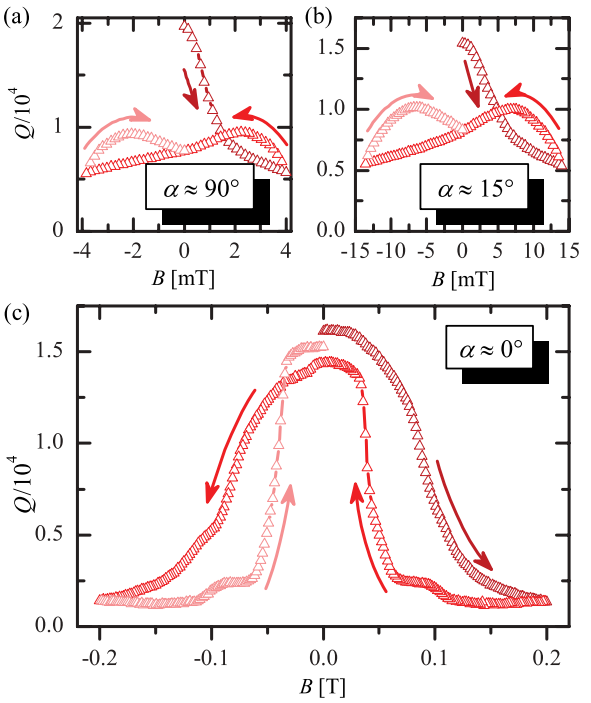

FIG. 11. (Color online) Typical measured hysteresis curves of the quality factor Q of the fundamental mode $n = 1$ (resonator 3+) during a full cycle of the magnetic field for three different angles (a) $\alpha = 90°$, (b) $\alpha \approx 15°$, and (c) $\alpha \approx 0°$ between resonator plane and applied field.

the quality factor increases and almost completely recovers to the original value of $Q(0)$. For negative fields we observe qualitatively the same behavior. It is also important to note that $Q^{\downarrow} \leqslant Q^{\Uparrow}$.

Interestingly, a comparison of measurement results with the theoretical curves presented in Sec. IV shows the best agreement with the prediction of the classical Bean model and not the NBI model; cf. Fig. 5. Although at first sight one would indeed expect the classical Bean model to be the adequate description for the flux density profile in this experimental situation (field parallel to a superconducting plane), one has to be careful with this interpretation for two reasons. First, one has to consider that the film thickness $d = 300$ nm is about three times the penetration depth ($\lambda_{\text{eff}} \approx 100$ nm) and, therefore, only 1.5 times the diameter of one Abrikosov vortex. Hence, the Bean model as a kind of a mean field theory might probably need a modification to properly describe the resonator losses in this case. The step-like structures in $Q(B)$ (e.g., at $B \approx \pm 0.1$ T) might reflect some kind of a discrete and nonsmooth flux entry into and exit out of the superconductor. Moreover, it is likely that the measured hysteresis is also partly the result of a small misalignment between the applied field and the resonator plane. At flux densities of $B \approx 100$ mT, an alignment error of only 0.5° already introduces a field of $\approx$1 mT perpendicular to the film, which is large enough to significantly reduce Q; cf. Fig. 11(a). Obviously, the hysteresis loop seems not to allow for reducing the microwave losses in the resonator if the magnetic field is applied close to parallel to the superconducting film.

VII. CONCLUSIONS

We experimentally investigated the properties of 3.3 GHz superconducting coplanar transmission line resonators in magnetic fields. In particular, we focused on resonators that were zero-field cooled to $T = 4.2$ K and then exposed to magnetic field cycles in the milli-Tesla range. We measured the resonance frequency f_{res} and quality factor Q of the resonators and found strong hysteresis effects, which on the mesoscopic scale are due to the presence of Abrikosov vortices in the superconducting film and their spatial redistribution during the field cycles. By using a simple model for the vortex-associated resonator losses, we shown that different combinations of microwave current and flux density distributions lead to characteristically different hysteresis loops. We find best agreement between experiment and theory for a current distribution that is strongly peaked at the resonator edges and with a modified Bean flux gradient for thin films, as described by Norris, Brandt, and Indenbom. We have also shown that the hysteresis may be used to improve the resonator performance for fixed values of applied magnetic field by proper choice of magnetic history. Accordingly, the resonance frequency can be tuned by about 1 MHz, i.e., for our resonators by a few zero-field linewidths at liquid Helium temperature. Both the reduction of the losses and the tunability of the frequency are found to be possible for resonators with and without antidots. Furthermore, we show that the hysteresis can also be found for higher modes $n = 2,3,4$ of the resonators and for angles between 90° and a few degrees between the field direction and the resonator plane. In the parallel field orientation, the hysteresis showed a very different behavior with presumably no possibility for a resonator improvement with magnetic history.

For many experiments in circuit quantum electrodynamics, superconducting resonators are operated in the Millikelvin and single photon regime. Hence, the effects presented here have to be investigated under these conditions in further studies. Still, there are no obvious reasons why the reported hysteresis effects should qualitatively change with decreasing temperature and power. Other parameters that are expected to change the nature of the hysteresis and that have to be considered for possible applications are the geometric dimensions of the transmission line and the thickness of the films, which together with the magnetic penetration depth have a strong influence on current distribution and flux density profile.

ACKNOWLEDGMENTS

This work has been supported by the Deutsche Forschungsgemeinschaft via the SFB/TRR 21 and by the European Research Council via SOCATHES. It was partly funded by the German Federal Ministry of Education and Research (Grant No. 01BQ1061). D.B. acknowledges support by the Evangelisches Studienwerk e.V. Villigst. M.K. acknowledges support by the Carl-Zeiss Stiftung. The authors thank Roger Wördenweber for fruitful discussions.

*daniel.bothner@uni-tuebingen.de

[1] C. P. Bean, Phys. Rev. Lett. **8**, 250 (1962).
[2] C. P. Bean, Rev. Mod. Phys. **36**, 31 (1964).
[3] A. Wallraff, D. I. Schuster, A. Blais, L. Frunzio, R.-S. Huang, J. Majer, S. Kumar, S. Girvin, and R. J. Schoelkopf, Nature (London) **431**, 162 (2004).
[4] M. Hofheinz *et al.*, Nature (London) **459**, 546 (2009).
[5] T. Niemczyk *et al.*, Nature Physics **6**, 772 (2010).
[6] L. DiCarlo *et al.*, Nature (London) **460**, 240 (2009).
[7] P. K. Day, H. G. LeDuc, B. A. Mazin, A. Vayonakis, and J. Zmuidzinas, Nature (London) **425**, 817 (2003).
[8] H. Wang *et al.*, Appl. Phys. Lett. **95**, 233508 (2009).
[9] P. Macha, S. H. W. van der Ploeg, G. Oelsner, E. Il'ichev, H.-G. Meyer, S. Wünsch, and M. Siegel, Appl. Phys. Lett. **96**, 062503 (2010).
[10] R. Barends, N. Vercruyssen, A. Endo, P. J. de Visser, T. Zijistra, T. M. Klapwijk, P. Diener, S. J. C. Yates, and J. J. A. Baselmans, Appl. Phys. Lett. **97**, 023508 (2010).
[11] T. Lindström, J. E. Healey, M. S. Colclough, C. M. Muirhead, and A. Y. Tzalenchuk, Phys. Rev. B **80**, 132501 (2009).
[12] P. Rabl, D. DeMille, J. M. Doyle, M. D. Lukin, R. J. Schoelkopf, and P. Zoller, Phys. Rev. Lett. **97**, 033003 (2006).
[13] A. Imamoglu, Phys. Rev. Lett. **102**, 083602 (2009).
[14] J. Verdú, H. Zoubi, C. Koller, J. Majer, H. Ritsch, and J. Schmiedmayer, Phys. Rev. Lett. **103**, 043603 (2009).
[15] K. Henschel, J. Majer, J. Schmiedmayer, and H. Ritsch, Phys. Rev. A **82**, 033810 (2010).
[16] P. Bushev *et al.*, Eur. Phys. J. D **63**, 9 (2011).
[17] J. Fortágh and C. Zimmermann, Science **307**, 860 (2005).
[18] P. Bushev, S. Stahl, R. Natali, G. Marx, E. Stachowska, G. Werth, M. Hellwig, and F. Schmidt-Kaler, Eur. Phys. J. D **50**, 97 (2008).
[19] C. Song, T. W. Heitmann, M. P. DeFeo, K. Yu, R. McDermott, M. Neeley, J. M. Martinis, and B. L. T. Plourde, Phys. Rev. B **79**, 174512 (2009).
[20] D. I. Schuster *et al.*, Phys. Rev. Lett. **105**, 140501 (2010).
[21] Y. Kubo, F. R. Ong, P. Bertet, D. Vion, V. Jacques, D. Zheng, A. Dréau, J.-F. Roch, A. Auffeves, F. Jelezko, J. Wrachtrup, M. F. Barthe, P. Bergonzo, and D. Esteve, Phys. Rev. Lett. **105**, 140502 (2010).
[22] C. Song, M. P. DeFeo, K. Yu, and B. L. T. Plourde, Appl. Phys. Lett. **95**, 232501 (2009).
[23] D. Bothner, T. Gaber, M. Kemmler, D. Koelle, and R. Kleiner, Appl. Phys. Lett. **98**, 102504 (2011).
[24] D. Bothner, C. Clauss, E. Koroknay, M. Kemmler, T. Gaber, M. Jetter, M. Scheffler, P. Michler, M. Dressel, D. Koelle, and R. Kleiner, Appl. Phys. Lett. **100**, 012601 (2012).
[25] C. Jooss, J. Albrecht, H. Kuhn, S. Leonhardt, and H. Kronmüller, Rep. Prog. Phys. **65**, 651 (2002).
[26] P. Lahl and R. Wördenweber, Appl. Phys. Lett. **81**, 505 (2002).
[27] W. T. Norris, J. Phys. D: Appl. Phys. **3**, 489 (1970).
[28] E. H. Brandt and M. Indenbom, Phys. Rev. B **48**, 12893 (1993).
[29] G. Hammer, S. Wuensch, M. Roesch, K. Ilin, E. Crocoll, and M. Siegel, Supercond. Sci. Technol. **20**, 408 (2007).
[30] P. Lahl and R. Wördenweber, IEEE Trans. Appl. Supercond. **13**, 2917 (2003).

[31]M. Bonura, E. Di Gennaro, A. Agliolo Gallitto, and M. Li Vigni, Eur. Phys. J. B **52**, 459 (2006).
[32]M. Bonura, A. Agliolo Gallitto, and M. Li Vigni, Eur. Phys. J. B **53**, 315 (2006).
[33]D. E. Oates, S.-H. Park, and G. Koren, Phys. Rev. Lett. **93**, 197001 (2004).
[34]M. Göppl, A. Fragner, M. Baur, R. Bianchetti, S. Filipp, J. M. Fink, P. J. Leek, G. Puebla, L. Steffen, and A. Wallraff, J. Appl. Phys. **104**, 113904 (2008).
[35]J. I. Gittleman and B. Rosenblum, J. Appl. Phys. **39**, 2617 (1968).
[36]E. H. Brandt, Phys. Rev. Lett. **67**, 2219 (1991).
[37]M. W. Coffey and J. R. Clem, Phys. Rev. Lett. **67**, 386 (1991).
[38]N. Klein, H. Chaloupka, G. Müller, S. Orbach, H. Piel, B. Rosa, L. Schultz, U. Klein, and M. Peiniger, J. Appl. Phys. **67**, 6940 (1990).
[39]A. I. Gubin, K. S. Ilin, S. A. Vitusevich, M. Siegel, and N. Klein, Phys. Rev. B **72**, 064503 (2005).
[40]A. G. Zaitsev, R. Schneider, R. Hott, Th. Schwarz, and J. Geerk, Phys. Rev. B **75**, 212505 (2007).
[41]M. A. Golosovsky, H. J. Snortland, and M. R. Beasley, Phys. Rev. B **51**, 6462 (1995).
[42]P. Lahl and R. Wördenweber, J. Appl. Phys. **97**, 113911 (2005).
[43]J. E. Healey, T. Lindström, M. S. Colclough, C. M. Muirhead, and A. Ya. Tzalenchuk, Appl. Phys. Lett. **93**, 043513 (2008).
[44]A. Palacios-Laloy, F. Nguyen, F. Mallet, P. Bertet, D. Vion, and D. Esteve, J. Low Temp. Phys. **151**, 1034 (2008).
[45]M. Sandberg, C. M. Wilson, F. Persson, T. Bauch, G. Johansson, V. Shumeiko, T. Duty, and P. Delsing, Appl. Phys. Lett. **92**, 203501 (2008).